Title
Single-molecule Taq DNA polymerase dynamics

Journal
Science Advances, 8(10)

ISSN
2375-2548

Authors
Turvey, Mackenzie W
Gabriel, Kristin N
Lee, Wonbae
et al.

Publication Date
2022-03-11

DOI
10.1126/sciadv.abl3522

CHEMISTRY

Single-molecule Taq DNA polymerase dynamics

Mackenzie W. Turvey[1]†, Kristin N. Gabriel[2]†, Wonbae Lee[1], Jeffrey J. Taulbee[1], Joshua K. Kim[3], Silu Chen[3], Calvin J. Lau[1], Rebecca E. Kattan[2], Jenifer T. Pham[3], Sudipta Majumdar[3], Davil Garcia[5], Gregory A. Weiss[2,3,4]*, Philip G. Collins[1]*

Taq DNA polymerase functions at elevated temperatures with fast conformational dynamics—regimes previously inaccessible to mechanistic, single-molecule studies. Here, single-walled carbon nanotube transistors recorded the motions of Taq molecules processing matched or mismatched template–deoxynucleotide triphosphate pairs from 22° to 85°C. By using four enzyme orientations, the whole-enzyme closures of nucleotide incorporations were distinguished from more rapid, 20-μs closures of Taq's fingers domain testing complementarity and orientation. On average, one transient closure was observed for every nucleotide binding event; even complementary substrate pairs averaged five transient closures between each catalytic incorporation at 72°C. The rate and duration of the transient closures and the catalytic events had almost no temperature dependence, leaving all of Taq's temperature sensitivity to its rate-determining open state.

INTRODUCTION

DNA polymerases catalyze reactions essential to life—DNA replication and repair (*1*). They incorporate incoming deoxynucleotide triphosphates (dNTPs) into a nascent DNA strand that is complementary to a single-stranded DNA (ssDNA) template. This capability makes DNA polymerases workhorses for molecular biology and biotechnology (*2*). In particular, the thermostable DNA polymerase from *Thermus aquaticus* (Taq) is widely used in the polymerase chain reaction (PCR) (*3*).

The simplest model for DNA polymerase function is a catalytic cycle between open and closed conformations (*1*, *4*). In the open conformation, dNTP and ssDNA template bind to sites on the enzyme's "fingers" and "thumb" domains, respectively (*5*). After substrate binding, the two domains come together to form a closed conformation that either rejects the dNTP or catalytically incorporates it into the nascent ssDNA (*4*, *6*). While this simple model is broadly accepted, fundamental questions about the fidelity-checking mechanism have motivated searches for additional intermediate conformations (*7*, *8*). How does fidelity checking occur in the open conformation before the dNTP and DNA template can coordinate? Alternatively, if fidelity checking is postponed until the catalytically active, closed conformation, then how are misincorporation rates of 10^{-6} errors per dNTP achieved? Early research hypothesized the necessity of partially closed, intermediate conformations where dNTP identification and mismatch rejection could occur before the closed conformation (*6*, *9*).

Over the past decade, multiple breakthroughs began to identify and characterize these intermediate conformations in Taq and homologous A-family DNA polymerases. In 2011, Wu and Beese (*10*) crystallized an "ajar" structure using a noncomplementary pairing and mutagenic modifications to stabilize the conformation. Independently, advances in single-molecule Förster resonance energy transfer (smFRET) inferred partially closed conformations from fluorescence emission populations (*8*, *11*, *12*) and developed a dynamic model of rapidly interconverting conformational populations influenced by complementarity (*13*, *14*). On the theoretical side, all-atom molecular dynamics (MD) advanced to produce the first detailed trajectories of closing and reopening transitions (*15*, *16*), followed by observations of interconversion dynamics among a diverse ensemble of atomic configurations (*17*, *18*). Together, this progress has revealed partially closed intermediates and dynamics between the open and closed conformations, but it has not directly observed the fidelity-checking mechanism nor resolved the debate over whether "conformational selection," "induced fitting," or a combination of the two is the best reductionist model (*8*, *19*–*26*). A broad diversity in the MD trajectories suggests that fidelity checking is more complex than a binary choice between two deterministic, concerted pathways.

Here, we contribute long-duration, single-molecule trajectories of Taq opening and closing upon either matched or mismatched dNTP-template pairs. Using a solid-state electronic technique with microsecond resolution, we monitored individual Taq molecules over minutes of activity, directly recording processive catalytic dNTP incorporations interspersed among 20-μs, noncatalytic closures. The results agree with the glimpses provided by smFRET measurements (*11*, *12*, *14*) and MD trajectories (*17*), detailing the timing with which Taq tests for complementarity by closing upon matched or mismatched dNTPs. A further advantage of the electronic technique is its compatibility with a wide range of temperatures; here, Taq's single-molecule activity was studied from 22° to 85°C to cover the range relevant for PCR.

To record these trajectories, we attached Taq molecules to field-effect transistors (FETs) composed of individual, single-walled carbon nanotubes (SWNTs; Fig. 1A). The technique has proven useful with other enzymes (*27*, *28*), including the Klenow fragment (KF) of DNA polymerase (*29*–*31*). Following methods similar to our previous work (*29*) and adopting the single-cysteine variants of Taq studied by Xu *et al.* (*32*), we used a pyrene-maleimide linker to bioconjugate individual Taq molecules to SWNT devices in four distinct orientations designed to transduce signals from the backside of Taq's intervening (R411C), palm (A814C), fingers (R695C), or thumb (E524C) domains (figs. S1 to S5). Here, the resultant enzyme-SWNT devices are each referred to as Taq domain (e.g., Taq-Intervening). Atomic

[1]Department of Physics and Astronomy, University of California, Irvine, Irvine, CA 92697-4575, USA. [2]Department of Molecular Biology and Biochemistry, University of California, Irvine, Irvine, CA 92697-3900, USA. [3]Department of Chemistry, University of California, Irvine, Irvine, CA 92697-2025, USA. [4]Department of Pharmaceutical Sciences, University of California, Irvine, Irvine, CA 92697-3958, USA. [5]Carbon Technology Inc., Irvine, CA 92619, USA.
*Corresponding author. Email: gweiss@uci.edu (G.A.W.); collinsp@uci.edu (P.G.C.)
†These authors contributed equally to this work.

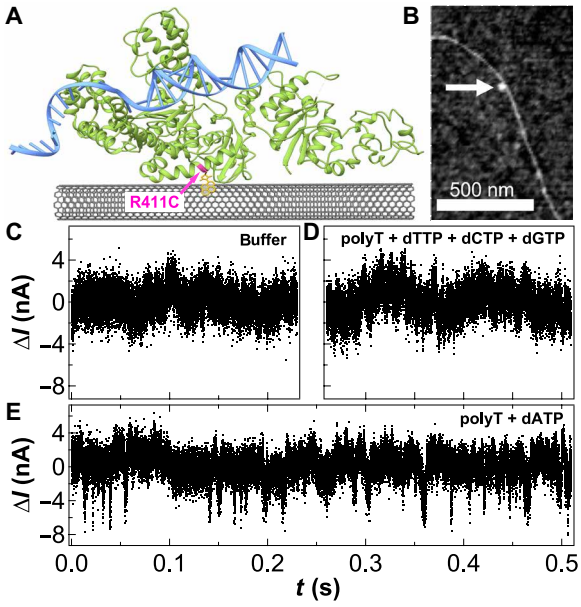

Fig. 1. A Taq-Intervening device schematic, atomic force microscopy (AFM) characterization, and sample signals generated at 72°C. (**A**) The Taq-Intervening device featured an individual Taq DNA polymerase (green) site-specifically bioconjugated to a SWNT through a cysteine in the intervening domain (residue R411C, pink) to a pyrene-maleimide linker molecule (yellow). (**B**) AFM image of a sample device with a single Taq attachment (white arrow). Representative $\Delta I(t)$ signals generated in solutions of (**C**) activity buffer, and polyT with (**D**) mismatched (dTTP + dCTP + dGTP) or (**E**) matched (dATP) dNTPs. Two-level excursions only occurred when polyT and complementary dNTPs were both present. Protein Data Bank: 1TAQ (*35*).

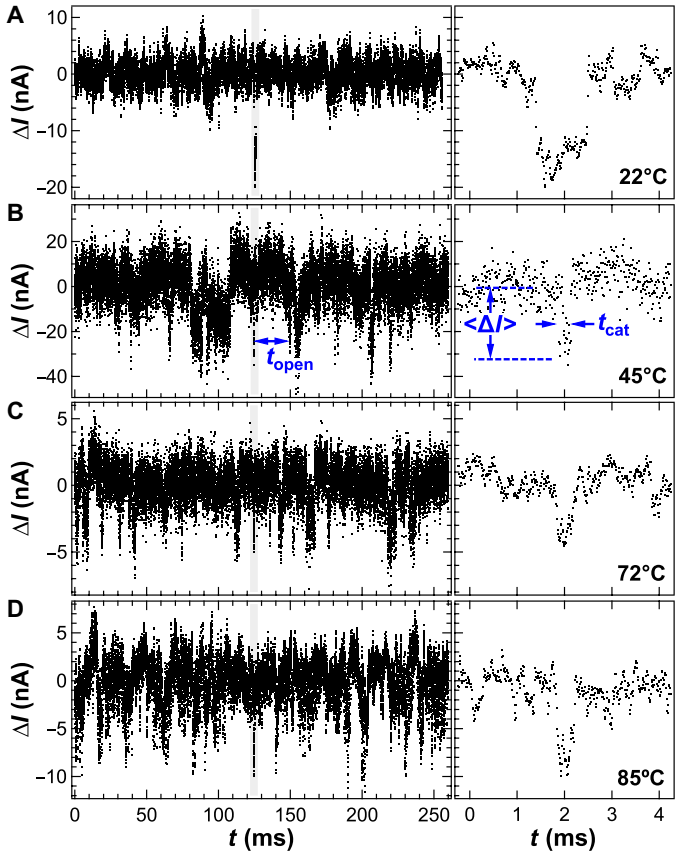

Fig. 2. Temperature dependence of $\Delta I(t)$ and individual catalytic closures. Taq-Intervening with matched dATP and polyT generated different rates of catalytic closures at (**A**) 22°, (**B**) 45°, (**C**) 72°, and (**D**) 85°C. While the rate of catalytic closures increased with temperature (left), the duration of individual catalytic closures stayed constant (gray highlights and right). For clarity, individual data points represent 10-μs intervals; 1-μs resolution data are shown in fig. S7.

force microscopy of an example Taq-Intervening device is shown in Fig. 1B and fig. S6. In each orientation, the movement of charged amino acid side chains closest to the SWNT electrostatically modulated the source-drain current $I(t)$, whereas more distant domains were screened by mobile ions in the Taq activity buffer [40 mM Hepes, 50 mM KCl, 5 mM $MgCl_2$ (pH 8.5)], which had a Debye screening radius of 1.2 nm (fig. S2). The electrical current as a function of time, $I(t)$, was recorded while Taq interacted with a solution of homopolymeric "polyT" DNA primer-template [4 nM poly$(dT)_{42}$ fused to an M13 priming site and annealed with M13 primer; table S1] and/or different dNTPs (typically 10 μM). The $\Delta I(t)$ signals presented here were high-pass filtered at 15 Hz to remove DC components of 10 to 500 nA and the lowest-frequency fluctuations from the raw $I(t)$ data. Materials and Methods provides a fuller description of the experimental methods for production and purification of each full-length Taq variant and SWNT FET fabrication, bioconjugation, and measurement.

RESULTS

Aside from being acquired at 72°C, the signals generated by Taq-Intervening devices were essentially identical to previous electrical measurements of KF (*33*). In activity buffer (Fig. 1C) or with mismatched dNTPs (Fig. 1D), $\Delta I(t)$ was a featureless band of $1/f$ noise. In the presence of matched dNTPs, additional two-level switching appeared (Fig. 1E and fig. S7). At 72°C, the average rate of Taq's two-level excursions below the baseline was 61 s^{-1}, effectively equal to Taq's catalytic rate k_{cat} at that temperature (*34*). Led by this agreement and the similarity to previous KF results (*29*), where event counting correctly enumerated DNA primer-template lengths (*31*), we assigned $\Delta I(t)$ to a two-state model of dNTP incorporations. The $\Delta I(t) = 0$ baseline corresponded to Taq's open conformation, and each excursion recorded one dNTP incorporation occurring in Taq's closed conformation. For brevity, we henceforth refer to these excursions as "catalytic closures."

Temperature dependence provided additional confirmation of the assignment of $\Delta I(t)$ excursions to Taq's catalytic closures. From 22° to 85°C, the average rate of catalytic closures increased exponentially from 4 to 96 s^{-1} (Fig. 2). While exact values varied from one molecule to another, the range of rates and the inferred activation energy of 11 kcal/mol (shown in fig. S8) was comparable to previous reports of k_{cat} (*36*–*39*). As in ensemble measurements (*36*, *38*), we observed a softening of the Arrhenius rate law above 50°C, where thermal fluctuations decrease Taq-dNTP and primer-template binding stabilities. At 95°C, $\Delta I(t)$ became disordered and not enumerable, but organized activity returned upon cooling devices below 85°C.

Figures 1 and 2 are short samples taken from continuous $\Delta I(t)$ records lasting no less than 5 min and, in some cases, as long as 45 min. At PCR temperatures, the full recordings contained thousands of

catalytic closures per minute, each of which could be resolved and individually characterized in the manner depicted in Fig. 2B. For quantitative statistical analysis, each catalytic closure was assigned a duration τ_{cat}, a waiting time before the closure τ_{open}, and an average amplitude $<\Delta I>$ measured from the event's instantaneous baseline. Transition times at the front and back step edges of each catalytic closure were also inspected but determined to be limited by the amplifier rise time (0.5 μs). Unlike previous work with T4 lysozyme, which directly observed finite transition times averaging 37 μs (*40*), most Taq open-to-closed transitions had sharp edges and rise times faster than 1 μs.

Figure 3 shows probability distribution functions for large populations of τ_{open} and τ_{cat} from Taq-Intervening activity at four temperatures. τ_{open} exhibited strong temperature dependence, consistent with previous ensemble work (*6*), whereas τ_{cat} was largely temperature independent. k_{cat} was essentially determined by the former, because τ_{open} was 100 to 1000 times longer than τ_{cat}. Consequently, Fig. 3A is a single-molecule representation of Taq's k_{cat} and its temperature dependence, illustrating the single-molecule, event-by-event composition of k_{cat} and its instantaneous variability. Solid lines in Fig. 3A depict single-exponential fits for a Poisson process with a single, rate-limiting step. The slope of each line equals the mean value of k_{cat} at each temperature; steepening τ_{open} distributions graphically illustrate Taq's increasing activity up to 85°C.

The τ_{open} distributions exceeded the exponential fits at longer durations, but this deviation occurred over many minutes of acquisition. Shorter subpopulations of τ_{open} fit single exponentials with minute-by-minute variations in slope. Similar variability was observed in τ_{cat}, causing its cumulative distributions to resemble double-exponential curves (Fig. 3B). This artificial stretching of single-exponential distributions can indicate external factors like temperature variation or dynamic disorder intrinsic to an enzyme

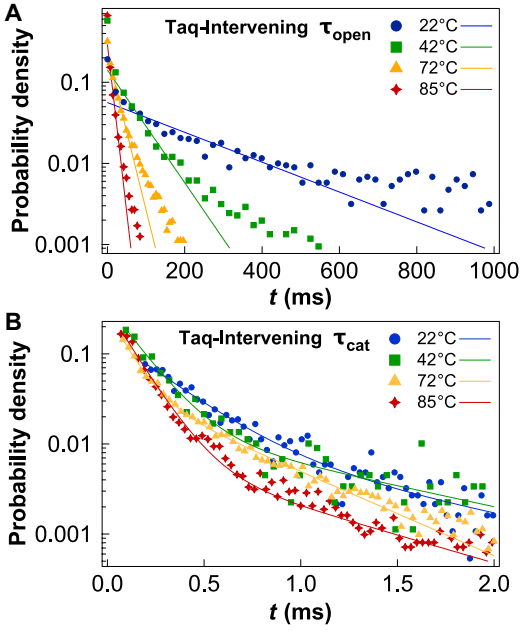

Fig. 3. Taq-Intervening open and closed durations processing matched substrate (polyT + dATP). (**A**) Probability distributions of the rate-determining waiting time, τ_{open}, with single-exponential fits. (**B**) Probability distributions of the catalytic closure durations, τ_{cat}, with double-exponential fits.

(*41*–*44*), but the latter explanation seems more likely because τ_{cat} had no other temperature sensitivity. Table 1 summarizes numeric values for the fits in Fig. 3 with the range (±σ) of single-exponential τ_{cat} fits that were observed experimentally at each temperature during extended recordings. Data from the ends of these ranges are responsible for the long tails in the cumulative distributions shown in Fig. 3.

Taq-Palm devices corroborated the findings from Taq-Intervening. The Taq-Palm orientation suffered from sparse activity, perhaps inhibited by its attachment to the SWNT FET, but otherwise minute-long bursts of $\Delta I(t)$ excursions had the same characteristics as Taq-Intervening (fig. S9). Even studied in detail, however, the single-molecule trajectories from Taq-Palm and Taq-Intervening devices only observed k_{cat} activity already well established by ensemble and smFRET studies. The palm and intervening domains participated in the enzyme's global transformations during catalysis (*32*), but these attachment sites were located too far from the incoming dNTPs to transduce the dynamic activity associated with complementarity checking (fig. S2). Studying those signals required new orientations that attached the SWNT FET directly to the fingers or thumb domains.

Taq-Fingers devices produced $\Delta I(t)$ signals with two distinct populations of events. The first population was identical to the Taq-Intervening catalytic closures, having the same τ_{cat} probability distribution and thermally activated rates k_{cat}, and only occurring in polyT solutions with matched dNTPs [e.g., 2′-deoxyadenosine 5′-triphosphate (dATP)]. The second population of events, on the other hand, appeared in $\Delta I(t)$ signals collected in both matched (Fig. 4A) and mismatched dNTPs (Fig. 4B). This population of events, which we term "transient closures," was also distinguished by an average duration $<\tau_{transient}> = 18 \pm 6$ μs, approximately eight times shorter than $<\tau_{cat}>$. In mismatched dNTPs (where transient closures were easiest to analyze because catalytic closures were absent), transient closures occurred at a mean rate $k_{transient} = 10 \pm 8\ s^{-1}$ with a single-exponential distribution of durations (Fig. 4C). Datasets acquired at 45°, 60°, and 75°C could not resolve any temperature dependence in the characteristics of these transient closures (fig. S10). As with catalytic closures, observing transient closures required the presence of both DNA primer-template and dNTP; these events disappeared in control measurements using buffer, polyT alone, or dNTPs alone (fig. S11). Similar signals were generated by Taq-Thumb devices (fig. S12).

In matched dNTPs, Taq-Fingers signals contained a mixture of the new transient closures along with the catalytic closures observed with Taq-Intervening. The two types of events overlapped in a biexponential distribution (Fig. 4C), making classification of individual events impossible in the 75- to 125-μs region where the two subpopulations had comparable probabilities. Overall, though, the subpopulations were distinguishable and easily identified with help from the single-population datasets. The longer-duration subpopulation of

Table 1. Taq-Intervening open and closed durations processing matched substrate (polyT + dATP).

T (°C)	$\tau_{open} \pm \sigma$ (ms)	*k* (s^{-1})	$\tau_{cat} \pm \sigma$ (ms)
22	236 ± 15	4	0.67 ± 0.41
42	62 ± 2	16	0.57 ± 0.33
72	16.4 ± 0.6	61	0.45 ± 0.15
85	10.4 ± 0.2	96	0.33 ± 0.09

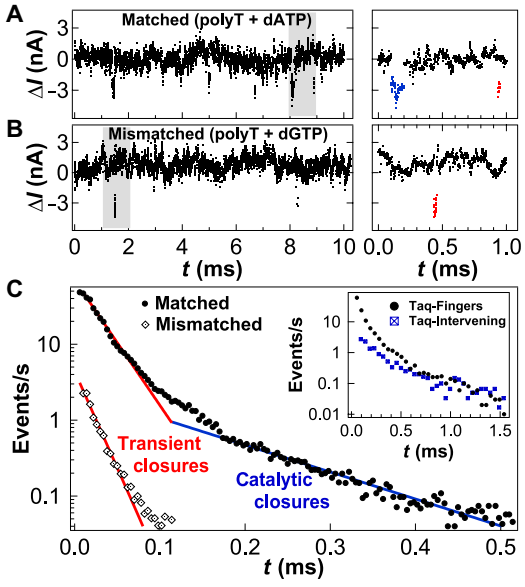

Fig. 4. Taq-Fingers activity in matched and mismatched dNTPs at 45°C. Taq-Fingers closures upon polyT with (**A**) matched dATP or (**B**) mismatched dGTP. Gray highlights the regions expanded at right with examples of individual catalytic closures (blue) and transient closures (red) at 1-μs resolution. Transient closures occurred in both matched dATP and mismatched dGTP, while catalytic closures only occurred with matched dATP. (**C**) Statistical distributions of closures per second in matched dATP (circles) and mismatched dGTP (diamonds) with 4-μs bin widths. The matched dATP data contained a combination of two types of events, whereas the mismatched dGTP only contained the transient closures. (Inset) On a longer time axis with 20-μs bins, the Taq-Fingers events denoted as catalytic closures overlapped the distribution of events measured with Taq-Intervening.

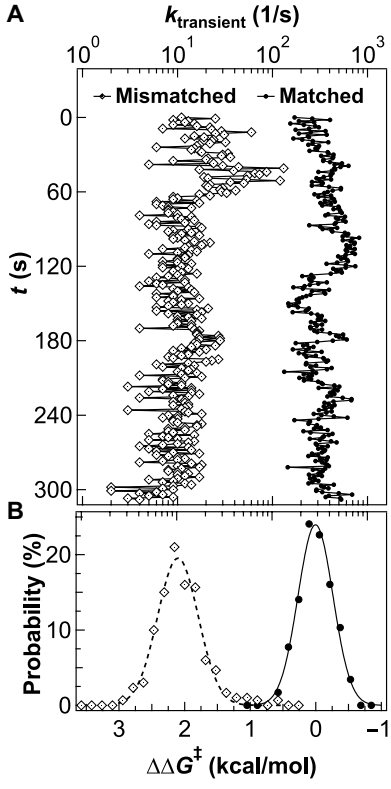

Fig. 5. Variable kinetics of Taq-Fingers transient closures. (**A**) Instantaneous rates calculated on 1-s intervals depict $k_{transient}$'s mean and range of variation with matched dATP (circles) or mismatched dGTP (diamonds). (**B**) Cumulative probability distributions on dual horizontal axes of rate (1/s, top) and relative energy (kcal/mol, bottom), overlaid with log-normal fits.

Taq-Fingers events overlapped perfectly with the catalytic closures measured with Taq-Intervening (Fig. 4C, inset), and the shorter-duration subpopulation overlapped with the transient closures observed with mismatched dNTPs. The sole difference among these comparisons was that the rate $k_{transient}$ rose from 10 s^{-1} in mismatched dNTPs to 280 ± 150 s^{-1} in matched dNTPs. To depict this difference quantitatively, Fig. 4C shows the matched and mismatched population distributions in units of events per second.

As noted above, single-exponential fits to the τ_{cat} and $\tau_{transient}$ distributions disguised the actual dynamics and variability in k_{cat} and $k_{transient}$. When calculated on 1-s intervals from single-molecule trajectories, both rates varied within a tenfold range. Figure 5 shows instantaneous $k_{transient}$ values (Fig. 5A) and the moment-to-moment accumulation of those values into log-normal probability distributions, with well-separated distributions for matched and mismatched dNTPs (Fig. 5B). The log-normal fitting indicates that $k_{transient}$ obeyed a thermodynamic rate equation $\ln(k_{transient}/k_0) = -\Delta G^{\ddagger}/k_B T$, where $\Delta G^{\ddagger}$ is the energy barrier for transient-closing motions, k_0 is an attempt rate, and k_B is Boltzmann's constant. Plotting $k_{transient}$ on a relative energy axis $\Delta\Delta G^{\ddagger}$ illustrates two important features. First, the distribution widths full width at half maximum = 0.65 ± 0.05 kcal/mol equaled 1 $k_B T$, showing that thermal fluctuations in $\Delta G^{\ddagger}$ governed the $k_{transient}$ variability. Figure S13 expands upon Fig. 5 with a comparison of $k_{transient}$ variability at 45°, 60°, and 72°C, demonstrating that the ~$k_B T$ width exceeded all other temperature dependence.

The second important feature of the $\Delta\Delta G^{\ddagger}$ axis in Fig. 5 is the energetic interpretation it provides for $k_{transient}$. The 30-fold difference between matched and mismatched $k_{transient}$ values is energetically summarized as a peak-to-peak energy difference of 2.1 ± 0.2 kcal/mol. This separation exactly matches the difference in binding affinities revealed by ensemble assays two decades ago (*6*, *9*, *45*, *46*). Thus, the preferential binding of matched dNTPs, well-accepted and established by ensemble measurements, reappeared with identical energetics when thousands of single-molecule events were fit to log-normal curves in Fig. 5.

Despite this one-to-one correspondence between dNTP binding and transient closures, the electronic technique did not sense dNTP binding directly. No $\Delta I(t)$ excursions were produced in the absence of template, although Taq binds dNTP in the absence of template. Therefore, we conclude that any $\Delta I(t)$ excursion observed electronically was not a binding event per se, but rather a closure of the Taq-template-dNTP complex induced subsequent to binding. Matched dNTPs bind at rates 30 times higher than unmatched dNTPs, and that difference manifested itself in the single-molecule data as a 30-fold increase of transient closures. This linear correspondence further suggests that mismatched dNTPs dissociate after a single transient closure. An efficient mismatch-rejection mechanism might operate in that manner to avoid multiple closure attempts on the same dNTP.

Other than the differences in rates and durations already noted, no other characteristics of the $\Delta I(t)$ excursions distinguished matched from mismatched dNTPs or transient closures from catalytic ones. Three hypotheses were given special attention in the data analysis.

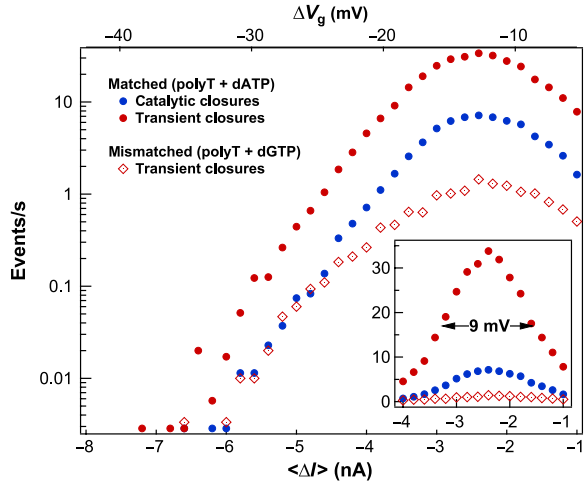

Fig. 6. Distributions of event amplitudes <Δ*I*> generated by Taq-Fingers. The amplitude <Δ*I*> of any event does not allow discrimination between matched (circles) and mismatched (diamonds) dNTPs nor between transient closures (red) and catalytic closures (blue). These four types of events had <Δ*I*> distributions with equal widths and peak positions. Here, event duration was used to separate events in matched dATP into either transient or catalytic closures. The top *x* axis provides a conversion of <Δ*I*> to its equivalent electrostatic gating ΔV_g, as determined from the device transconductance dI/dV_g. (**Inset**) Same distributions on a linear scale, showing the full width at half maximum of 9 mV.

First, the $\tau_{transient}$ and τ_{cat} events generated by Taq-Fingers were uniformly intermixed in dATP without evidence of bunching or sequencing, as if both were independent, memoryless Poisson processes. For instance, τ_{cat} events observed with Taq-Fingers had identical timing and statistics to those observed with Taq-Intervening. Second, the $\tau_{transient}$ durations were the same for matched dATP and mismatched 2′-deoxyguanosine 5′-triphosphate (dGTP), ruling out event duration as a possible direct measurement of any fidelity-checking step. Third, the transient and catalytic closures had identical distributions of the signal amplitude observed for Taq-Fingers (Fig. 6). This latter observation is important because <Δ*I*> is electrostatically transduced by motions of charged amino acids near the attachment site. Because <Δ*I*> did not distinguish matched and mismatched dNTPs or catalytic closures from transient closures, the SWNT FET was registering the same degree of amino acid motion in all three cases. On the other hand, <Δ*I*> differed between Taq-Fingers, Taq-Intervening, and the other two orientations, reflecting the different compositions of signal-generating amino acids at each attachment site.

DISCUSSION

Historically, the preferential binding of matched dNTPs has generated many questions about fidelity-checking mechanisms in polymerases. Before binding dNTP, Taq sits in an open conformation with the templating base far from the dNTP binding site on the fingers domain. Researchers have questioned how a preference for one dNTP over another arises and transmits to the fingers domain (*6*, *9*, *45*). Ultrashort finger-closing transients or partially closed intermediate conformations have both been proposed as possible keys to such a mechanism (*12*). However, the dynamical time scales of these transients have been proven too brief for direct observation by smFRET (*13*, *14*, *47*). Modern MD simulations have reproduced the 2 kcal/mol preference for binding matched dNTPs (*15*, *17*, *18*), but only in closed or partially closed conformations and with submicrosecond time scales. Nevertheless, transients into and through intermediates have grown to be widely anticipated feature of Taq's dynamics.

In the present work, the observations described above lead us to conclude that Δ*I*(*t*) was not sensitive to Taq's partially closed conformations, especially any conformation key to fidelity checking (*12*). Instead, fidelity checking completely preceded the motions detected by Δ*I*(*t*), leading to the one-to-one correspondence between binding and closure and the lack of any <Δ*I*> difference between catalytic closures and transient ones. Close inspection of Taq's structure in the Taq-Fingers orientation suggests that one charged amino acid (D655) generated the Δ*I*(*t*) excursions but only when Taq closed fully and not in the partially closed conformation reported by Wu and Beese (*10*). Therefore, we conclude that Δ*I*(*t*) excursions reported the fully closed conformation and that Δ*I*(*t*) was not sensitive to partially closed conformations. Distinguishing those may require carefully designed mutations in future experiments, as well as higher bandwidths if the event durations are less than 1 μs.

Even without resolving intermediate conformations, the detailed observation of transient closures remains important in two ways. First, transient closures occurred with matched dNTPs and this was an unexpected dynamic. At 72°C, there were approximately five transient closures for every catalytic closure ($k_{transient}/k_{cat} = 5$). No model has suggested that polymerase might pass a fidelity checkpoint with a matched dNTP and yet still proceed through multiple noncatalytic closures. When the temperature was lowered, transient closures continued to occur at $k_{transient} = 280\ s^{-1}$, while the number of catalytic closures $1/k_{cat}$ decreased exponentially, filling the entire τ_{open} duration with transient closures. This free-running process requires revisions to the linear, multistep diagrams often used to represent Taq's catalytic cycle (*9*, *48*).

Second, transient closures were observed upon binding mismatched dNTPs. Again, the premise of a fidelity checkpoint is to reduce misincorporations by reducing closures upon mismatched dNTPs. Here, Taq appears to have fully closed once upon every dNTP binding event, whether matched or mismatched. Closing upon mismatched dNTPs after fidelity checking may be counterintuitive, but that kind of motion has been inferred from the analysis of smFRET transition probabilities (*14*) and directly seen in MD trajectories (*17*). The MD research, in particular, has suggested that the mismatch-rejection mechanism might need to follow a trajectory in which Taq briefly accesses the closed conformation after the fidelity check and on the way to reopening and dNTP dissociation. In this type of cycle, each mismatched dNTP binding event is followed by one transient closure with a one-to-one correspondence as reported here.

Last, the observed dynamics lead us to propose a previously undescribed sequence in which matched dNTPs also dissociate after every transient closure. While expected for mismatched dNTPs, frequent dissociation of matched dNTPs is contrary to the optimization of catalytic rate. Nevertheless, our proposal is based on two observations. First, if Taq executes one transient closure per binding and dissociation cycle with mismatched dNTP, then it must perform a similar cycle with matched dNTPs to produce a $k_{transient}$ ratio that matches the ratio of ensemble binding rates. Otherwise, if matched dNTPs remained bound through multiple transient closures, then the $k_{transient}$ ratio would be multiple times the 30:1 ratio of binding events. Second, the Δ*I*(*t*) recordings with matched dNTPs show that transient closures filled τ_{open} and occurred at a temperature-insensitive,

constant rate $k_{transient}$. These data suggest a rapid and continuous cycle of dNTP binding, closure, and dissociation that repeats indefinitely while awaiting the completion of some other, thermally activated and rate-limiting step.

This type of continuous cycling does not fit the common schemes used to represent Taq's catalytic cycle with matched dNTPs. In most of these schemes (*9*, *48*), dNTP binding is one of a linear series of steps that occurs during τ_{open} and that proceeds directly to catalysis after successful fidelity checking. If τ_{open} is instead filled with a free-running, parallel cycle of dNTP binding, closure, and dissociation, then that cycle could require rethinking the schemes for Taq's steps and revisiting the interpretation of ensemble experiments where rate constants were extracted by assuming a linear scheme.

Transient closures with matched dNTPs may reflect misalignment of the molecular orbitals required for bond formation and breakage. The observation of multiple transient closures per catalytic closure may reflect some of Taq's dynamical interconversions as it previews the closed conformation and cycles back to open or partially open conformations to achieve correct template positioning, dNTP orientation, or alignment of active site and substrate functionalities, including Mg^{2+}. On the other hand, the $\tau_{transient}$ distributions with matched and mismatched dNTPs had identical durations and they both fit single-step Poisson distributions, so any rearrangement or repositioning was not occurring during the transient closure. Furthermore, closures lasting less than 5 μs were not counted here, leaving many additional opportunities for another population of the submicrosecond dynamics predicted by MD simulations (*16*, *18*). Once the molecular orbital alignment is correct, a catalytic closure can proceed (*7*) with the global conformational changes that extend to the palm and intervening domains (*32*). Figure S14 depicts a likely sequence of transient closures and catalytic closures among the mechanistic steps of the catalytic sequence.

This work opens frontiers in protein engineering and biophysics. The conceptual separation of Taq's catalytic cycle into a thermally activated step and temperature-independent motions offers a successful paradigm for the evolution of high-temperature enzymes. Directed evolution of industrially important enzymes could benefit from exploiting this paradigm to achieve Taq's catalytic rate acceleration at elevated temperatures. Such capabilities are notoriously hard to engineer by standard experimental and computational approaches (*49*, *50*). Furthermore, the dynamics of DNA replication is merely one case of an important but complex chemical process challenging state-of-the-art biophysical techniques. More broadly, enzyme evolution, optimization, and engineering could all benefit from the ability to track single-molecule chemical trajectories indefinitely with microsecond resolution. The added benefits of operating over a wide temperature range or with solvent compatibility make the solid-state technique of single-molecule electronics a promising approach to reveal timing, sequence, and dynamic kinetics in a wide range of systems.

MATERIALS AND METHODS

Materials

Reagents purchased commercially include the following: cell lines (StrataGene), kanamycin (Carbosynth), isopropyl-β-D-thiogalactopyranoside (IPTG; Carbosynth), glycine (Bio Basic), and Ni-IMAC (immobilized metal affinity chromatography) resin (Bio-Rad Laboratories). All other chemicals were supplied by Fisher Scientific or Thermo Fisher Scientific. Supplies purchased commercially include the following: 0.22-μm vacuum filter (Genesee Scientific), 3.5K molecular weight cutoff (MWCO) 0.1-ml Slide-A-Lyzer mini dialysis device (Thermo Fisher Scientific), and Amicon Ultra 0.5-ml centrifuge filter (Fisher Scientific). All reagents and supplies were used as received. All solutions were sterile-filtered or autoclaved before use. Kits and services purchased commercially include the following: Q5 site-directed mutagenesis (New England Biolabs), QIAprep spin miniprep kit (Qiagen), Pierce bicinchoninic acid (BCA) assay kit (Thermo Fisher Scientific), and DNA sequencing (Genewiz).

Methods

Mutagenesis of Taq

A pET28c plasmid for ligation-independent cloning containing an open reading frame (ORF) encoding Taq fused to an N-terminal His_6 peptide epitope was mutated to abolish the polymerase's exonuclease activity (G46D) and introduce a single cysteine (R411C, E524C, R695C, or A814C) (table S2). Q5 site-directed mutagenesis was applied according to the manufacturer's instructions using Q5 Hot Start High-Fidelity DNA Polymerase and the appropriate oligos, Oligo1 to Oligo10 (table S1). The Kinase, Ligase, and DpnI mix (KLD mix) (5 μl) was transformed into TOP10 *Escherichia coli*–competent cells, and transformants were plated on a kanamycin-supplemented (50 μg/ml) agar plate before incubation at 37°C overnight. Five single colonies were selected to inoculate 4 ml of 2YT medium in a 15-ml culture tube supplemented with kanamycin (50 μg/ml). The seed cultures were incubated at 37°C with shaking at 225 rpm for 8 to 12 hours. Plasmid DNA was isolated using the QIAprep spin miniprep kit according to the manufacturer's instructions. The successful subcloning of the ORF of the Taq variants was checked via DNA sequencing using the appropriate oligos, Oligo11 to Oligo14 (table S1).

Protein expression and purification

Protein expression and purification was conducted using procedures previously described (*30*, *51*), with modifications as follows. The plasmid encoding each Taq variant was transformed via heat shock into competent BL21 Star (DE3) *E. coli*. A single colony was transferred to LB medium (25 ml) supplemented with kanamycin (50 μg/ml) and incubated at 37°C for 10 to 16 hours. An aliquot of the starter culture (10 ml) was transferred to LB medium (1 liter of LB in a 4-liter baffled flask). After reaching an optical density at 600 nm of ~0.4, the culture was induced through addition of IPTG (1 mM final concentration) before incubation, with shaking (225 rpm) at 37°C for 2 hours. The cells were centrifuged and the cell pellet and resuspended in lysis buffer [50 mM tris-HCl, 25 mM KCl, 50 mM glucose, 0.25% Tween 20, 10 mM β-Mercaptoethanol (BME), 1 mM phenylmethylsulfonyl fluoride (pH 7.8), and protease inhibitor cocktail]. Following sonication for 12 min (1-s pulse on and 3-s pulse off), deoxyribonuclease (DNase) was added to the cell lysate, and the solutions was incubated at 37°C for 30 min to eliminate DNA bound to the polymerase. Heating at 70°C for 30 min deactivated the DNase. The DNase-treated lysate was subjected to centrifugation (26,892 relative centrifugal force, 45 min, 4°C). The supernatant was incubated with charged Ni–nitrilotriacetic acid resin and bound overnight on a shaker (150 rpm at 4°C). The resin was loaded onto a column and subject to washes [50 mM tris-HCl, 25 mM KCl, 50 mM glucose, 0.25% Tween 20, 10 mM BME (pH 7.9)] with a concentration gradient of imidazole (wash buffer supplemented with 25 to 250 mM imidazole). After pooling and concentrating (by microconcentration with a 50-kDa MWCO), the eluted protein was further purified by size exclusion chromatography (Superdex 200 pg, 16/600 at a flow rate of 1.0 ml/min)

in activity buffer [40 mM Hepes, 50 mM KCl, 5 mM $MgCl_2$ (pH 8.5)]. The eluted fractions were collected and visualized by 12% SDS–polyacrylamide gel electrophoresis (fig. S4). For single-molecule measurements on SWNT devices, the purified recombinant protein was dialyzed using 3.5K MWCO 0.1-ml Slide-A-Lyzer mini dialysis device into attachment buffer [40 mM Hepes, 50 mM KCl, 5 mM $MgCl_2$ (pH 6.5)]. The protein concentration was determined by a BCA assay using the enzyme's estimated MW (www.expasy.org). For storage, the purified recombinant protein was dialyzed into storage buffer [20 mM tris-HCl, 100 mM KCl, 0.1 mM EDTA, 1 mM dithiothreitol, 0.5% Tween 20, 10% glycerol (pH 7.4)] and maintained to −80°C.

Ensemble activity assays

Before bioconjugation to SWNTs, Taq activity was examined using previously described ensemble activity assays (*30*, *51*), using Oligo15 and polyT or Oligo16 (table S1). The high-performance liquid chromatography–purified oligos were solubilized in water to 100 μM and hybridized to the template through annealing from 45° to 5°C with a 5°C temperature decrease every 5 min. The positive control reactions contained the Taq variant (2 μM), dATP (100 μM), and DNA template-primer (5 μM) in 1× Taq Reaction Buffer [20 mM tris-HCl, 50 mM KCl, 5 mM $MgCl_2$ (pH 8.3)]. The negative control reaction omitted Taq. Reactions were incubated at 72°C for 1 hour, before the addition of SYBR Green Nucleic Acid I stain, and then visualized by electrophoresis using 5% high-resolution agarose gel. Gels were imaged using a Typhoon scanner at 256 nm. A representative ensemble activity assay is shown in fig. S5.

Fabrication and measurement of SWNT FETs

SWNT FET devices were fabricated using techniques described previously (*29*). In brief, SWNTs were grown via chemical vapor deposition (CVD) from $Fe_{30}Mo_{84}$ catalyst seeds (*52*). The $Fe_{30}Mo_{84}$ catalyst nanoparticles were confined to Al_2O_3 islands photolithographically defined on a 4″ p++ silicon wafer with a 250-nm thermal oxide (Silicon Quest International). A fast-heating CVD recipe facilitated growth of approximately one straight, 100-μm-long SWNT per island. Immediately after growth, the wafer was baked in air (315°C, 30 min) to remove excess amorphous carbon, annealed (95%/5% flowing Ar/H_2 at 600°C, 60 min), and given a 15-nm protective Al_2O_3 coating by atomic layer deposition (Savannah S200, Cambridge NanoTech). Electrodes were defined by lithographically patterning a bilayer resist (S1808 on LOR-A1), selectively etching the Al_2O_3 (Transetch-N, Transene), e-beam evaporating 10-nm Pt and 40-nm Ni, and lifting off the resist (Remover PG, MicroChemicals). Devices were then passivated with poly(methyl methacrylate) (PMMA), with a small opening defined over each 2-μm SWNT channel by e-beam lithography. In the preferred protocol, devices were individually etched in Transetch-N to remove the protective Al_2O_3 in this windowed region immediately before biofunctionalization.

Biofunctionalization of the newly exposed channel proceeded in two stages. First, the device was soaked in a solution of 100 pM pyrene-maleimide diluted in 1 μM of pyrene in ethanol for 2 min to coat the SWNT surface with a monolayer of pyrene and pyrene-maleimide linkers. Excess pyrene was then gently rinsed away with ethanol for 2 min in a drop-by-drop fashion. Next, the device was submerged in flowing attachment buffer [40 mM Hepes, 50 mM KCl, 5 mM $MgCl_2$ (pH 6.5)] for 10 min to equilibrate the surface. For bioconjugation, the device was incubated in a solution of the same buffer with 4 nM Taq for 5 min, followed by 10 min of continuous rinsing with buffer to remove nonspecific protein. This protocol was optimized to yield approximately one Taq attachment per 2 μm of SWNT, which in our geometry equaled one active, single-molecule SWNT FET device for every pair of devices prepared (fig. S6). Figure S15 summarizes the measurements done with all four Taq variants and the types of signals observed in each case.

Before measurements, devices were mounted in a holder, wire-bonded, and compressed with a polydimethylsiloxane (PDMS) gasket. To achieve a proper seal between the PDMS and PMMA surface of the device, the PDMS gasket was sonicated in 80% ethanol and 20% isopropanol for 10 min before being clamped in place. A 100-μm-wide microfluidic channel in the PDMS confined the liquid solutions to flow over the exposed SWNT FET device. The potential of the liquid was controlled with Pt counter electrodes and Ag/AgCl reference electrodes mounted in the fluid inlets and outlets.

During electrical measurements, electrodes were controlled and monitored using National Instruments data acquisition hardware (PCI-6281) and LabVIEW 2018 software. A transimpedance current preamplifier with 10^7 V/A gain (DHPCA-100 with 0.55-μs rise time, or DLPCA-200 with 2.5-μs rise time, FEMTO) was used to bias the drain electrode (20 to 100 mV) and measure the source-drain current $I(t)$. The Pt counter electrode was set to electrostatically gate the SWNT near the middle of its linear operating range (typically −200 mV with respect to Pt), and then, signals were continuously digitized and stored at 2 MHz.

Statistical analysis

To isolate and analyze enzyme-induced $I(t)$ signals, a denoising filter was implemented with the LabVIEW 2018 wavelet analysis library. Two parallel, nonadaptive bandpass filters used Haar wavelets with garrote thresholding from 66 ms to 256 μs for a low-noise output channel or from 66 ms to 8 μs for a sharper-edged, high-frequency output channel. Figure S7 shows an example of raw $I(t)$ and the resulting filtered, high-frequency output channel. After denoising, an adaptive thresholding filter was applied to both channels to identify individual events, excluding fluctuations with durations ≤4 μs to avoid counting external noise sources.

After identification, each event was individually characterized. In addition to the event duration and mean event amplitude reported here, tabulated parameters included total variation, kurtosis, and frequency components calculated from both the raw signal and the denoised outputs. No features distinguished transient closures from catalytic closures except for their durations, and the duration distribution was smooth and continuous when both present in a dataset. Categorization into transient and catalytic subsets was therefore guided by biexponential fitting and comparison against single-exponential distributions, as depicted in Fig. 4C. For quantitative statistical analysis, nonoverlapping subsets were artificially divided into events lasting <75 μs (brief events) or >125 μs (long events), ignoring the indeterminate events in between. This definition of subsets introduced systematic undercounting of event frequencies. It also limited our pursuit of quantitative comparisons among the different Taq mutants.

We note that the 4-μs noise cutoff caused the analysis to ignore very short fluctuations and to introduce systematic error into the enumeration of rates. The cutoff truncates no less than 20% of events in a Poisson process having a mean duration $\langle\tau\rangle = 18$ μs, which was the experimental value for transient closures. The same cutoff truncates only 3% of events in a Poisson process with $\langle\tau\rangle = 150$ μs, which was a typical value for catalytic closures. All $k_{transient}$ and k_{cat} rates stated here are based on events enumerated by the analysis, without any adjustment to account for this systematic undercounting.

SUPPLEMENTARY MATERIALS

Supplementary material for this article is available at https://science.org/doi/10.1126/sciadv.abl3522

REFERENCES AND NOTES

1. G. Maga, in *Reference Module in Biomedical Sciences* (Elsevier Inc., 2019), pp. 376–378.
2. J. Aschenbrenner, A. Marx, DNA polymerases and biotechnological applications. *Curr. Opin. Biotechnol.* **48**, 187–195 (2017).
3. R. K. Saiki, D. H. Gelfand, S. Stoffel, S. J. Scharf, R. Higuchi, G. T. Horn, K. B. Mullis, H. A. Erlich, Primer-directed enzymatic amplification of DNA with a thermostable DNA polymerase. *Science* **239**, 487–491 (1988).
4. Y. Li, S. Korolev, G. Waksman, Crystal structures of open and closed forms of binary and ternary complexes of the large fragment of *Thermus aquaticus* DNA polymerase I: Structural basis for nucleotide incorporation. *EMBO J.* **17**, 7514–7525 (1998).
5. S. H. Eom, J. Wang, T. A. Steitz, Structure of Taq polymerase with DNA at the polymerase active site. *Nature* **382**, 278–281 (1996).
6. P. J. Rothwell, V. Mitaksov, G. Waksman, Motions of the fingers subdomain of Klentaq1 are fast and not rate limiting: Implications for the molecular basis of fidelity in DNA polymerases. *Mol. Cell* **19**, 345–355 (2005).
7. B. Holzberger, M. G. Pszolla, A. Marx, H. M. Möller, KlenTaq DNA polymerase adopts unique recognition states when encountering matched, mismatched, and abasic template sites: An NMR study. *Chembiochem* **13**, 635–639 (2012).
8. P. J. Rothwell, W. J. Allen, E. Sisamakis, S. Kalinin, S. Felekyan, J. Widengren, G. Waksman, C. A. M. Seidel, DNTP-dependent conformational transitions in the fingers subdomain of Klentaq1 DNA polymerase: Insights into the role of the "nucleotide-binding" state. *J. Biol. Chem.* **288**, 13575–13591 (2013).
9. C. M. Joyce, S. J. Benkovic, DNA polymerase fidelity: Kinetics, structure, and checkpoints. *Biochemistry* **43**, 14317–14324 (2004).
10. E. Y. Wu, L. S. Beese, The structure of a high fidelity DNA polymerase bound to a mismatched nucleotide reveals an "Ajar" intermediate conformation in the nucleotide selection mechanism. *J. Biol. Chem.* **286**, 19758–19767 (2011).
11. Y. Santoso, C. M. Joyce, O. Potapova, L. Le Reste, J. Hohlbein, J. P. Torella, N. D. F. Grindley, A. N. Kapanidis, Conformational transitions in DNA polymerase I revealed by single-molecule FRET. *Proc. Natl. Acad. Sci. U.S.A.* **107**, 715–720 (2010).
12. S. Y. Berezhna, J. P. Gill, R. Lamichhane, D. P. Millar, Single-molecule Förster resonance energy transfer reveals an innate fidelity checkpoint in DNA polymerase I. *J. Am. Chem. Soc.* **134**, 11261–11268 (2012).
13. G. W. Evans, J. Hohlbein, T. Craggs, L. Aigrain, A. N. Kapanidis, Real-time single-molecule studies of the motions of DNA polymerase fingers illuminate DNA synthesis mechanisms. *Nucleic Acids Res.* **43**, 5998–6008 (2015).
14. J. Hohlbein, A. N. Kapanidis, in *Methods in Enzymology* (Elsevier Inc., 2016), vol. 581, pp. 353–378.
15. B. R. Miller, C. A. Parish, E. Y. Wu, Molecular dynamics study of the opening mechanism for DNA polymerase I. *PLOS Comput. Biol.* **10**, e1003961 (2014).
16. B. R. Miller III, L. S. Beese, C. A. Parish, E. Y. Wu, The closing mechanism of DNA polymerase I at atomic resolution. *Structure* **23**, 1609–1620 (2015).
17. M. Meli, M. Sustarsic, T. D. Craggs, A. N. Kapanidis, G. Colombo, DNA polymerase conformational dynamics and the role of fidelity-conferring residues: Insights from computational simulations. *Front. Mol. Biosci.* **3**, 20 (2016).
18. A. V. Yeager, K. Humphries, E. Farmer, G. Cline, B. Miller, A. Yeager, B. R. Miller III, Investigation of nascent base pair and polymerase behavior in the presence of mismatches in DNA polymerase I using molecular dynamics. *J. Chem. Inf. Model.* **58**, 338–349 (2017).
19. R. Radhakrishnan, K. Arora, Y. Wang, W. A. Beard, S. H. Wilson, T. Schlick, Regulation of DNA repair fidelity by molecular checkpoints: "Gates" in DNA polymerase β's substrate selection. *Biochemistry* **45**, 15142–15156 (2006).
20. B. R. Prasad, S. C. L. Kamerlin, J. Florián, A. Warshel, Prechemistry barriers and checkpoints do not contribute to fidelity and catalysis as long as they are not rate limiting. *Theor. Chem. Acc.* **131**, 1288 (2012).
21. I. Wong, S. S. Patel, K. A. Johnson, An induced-fit kinetic mechanism for DNA replication fidelity: Direct measurement by single-turnover kinetics. *Biochemistry* **30**, 526–537 (1991).
22. K. Datta, A. J. Wowor, A. J. Richard, V. J. Licata, Temperature dependence and thermodynamics of klenow polymerase binding to primed-template DNA. *Biophys. J.* **90**, 1739–1751 (2006).
23. S. Kirmizialtin, V. Nguyen, K. A. Johnson, R. Elber, How conformational dynamics of DNA polymerase select correct substrates: Experiments and simulations. *Structure* **20**, 618–627 (2012).
24. B. R. Prasad, A. Warshel, Prechemistry versus preorganization in DNA replication fidelity. *Proteins* **79**, 2900–2919 (2011).
25. J.-P. Changeux, S. Edelstein, Conformational selection or induced fit? 50 years of debate resolved. *F1000 Biol. Rep.* **3**, 19 (2011).
26. A. J. Mulholland, A. E. Roitberg, I. Tuñón, Enzyme dynamics and catalysis in the mechanism of DNA polymerase. *Theor. Chem. Acc.* **131**, 1–4 (2012).
27. Y. Choi, I. S. Moody, P. C. Sims, S. R. Hunt, B. L. Corso, I. Perez, G. A. Weiss, P. G. Collins, Single-molecule lysozyme dynamics monitored by an electronic circuit. *Science* **335**, 319–324 (2012).
28. P. C. Sims, I. S. Moody, Y. Choi, C. Dong, B. L. Corso, O. T. Gul, P. G. Collins, G. A. Weiss, Electronic measurements of single-molecule catalysis by cAMP-dependent protein kinase A. *J. Am. Chem. Soc.* **135**, 7861–7868 (2013).
29. T. J. Olsen, Y. Choi, P. C. Sims, O. T. Gul, B. L. Corso, C. Dong, W. A. Brown, P. G. Collins, G. A. Weiss, Electronic measurements of single-molecule processing by DNA polymerase I (Klenow fragment). *J. Am. Chem. Soc.* **135**, 7855–7860 (2013).
30. K. M. Pugliese, O. Tolga Gul, Y. Choi, T. J. Olsen, P. C. Sims, P. G. Collins, G. A. Weiss, Processive incorporation of deoxynucleoside triphosphate analogs by single-molecule DNA polymerase I (Klenow fragment) nanocircuits. *J. Am. Chem. Soc.* **137**, 9587–9594 (2015).
31. O. T. Gül, K. M. Pugliese, Y. Choi, P. C. Sims, D. Pan, A. J. Rajapakse, G. A. Weiss, P. G. Collins, Single molecule bioelectronics and their application to amplification-free measurement of DNA lengths. *Biosensors* **6**, 29 (2016).
32. C. Xu, B. A. Maxwell, Z. Suo, Conformational dynamics of *Thermus aquaticus* DNA polymerase I during catalysis. *J. Mol. Biol.* **426**, 2901–2917 (2014).
33. Y. Choi, T. J. Olsen, P. C. Sims, I. S. Moody, B. L. Corso, M. N. Dang, G. A. Weiss, P. G. Collins, Dissecting single-molecule signal transduction in carbon nanotube circuits with protein engineering. *Nano Lett.* **13**, 625–631 (2013).
34. D. H. Gelfand, in *PCR Technology*, H. A. Erlich, Ed. (Stockton Press, Palgrave Macmillan, 1989), pp. 17–22.
35. Y. Kim, S. H. Eom, J. Wang, D. S. Lee, S. W. Suh, T. A. Steitz, Crystal structure of Thermus aquaticus DNA polymerase. *Nature* **376**, 612–616 (1995).
36. A. Chien, D. B. Edgar, J. M. Trela, Deoxyribonucleic acid polymerase from the extreme thermophile *Thermus aquaticus*. *J. Bacteriol.* **127**, 1550–1557 (1976).
37. M. A. Innis, K. B. Myambo, D. H. Gelfand, M. A. D. Brow, DNA sequencing with *Thermus aquaticus* DNA polymerase and direct sequencing of polymerase chain reaction-amplified DNA. *Proc. Natl. Acad. Sci. U.S.A.* **85**, 9436–9440 (1988).
38. A. Langer, M. Schräml, R. Strasser, H. Daub, T. Myers, D. Heindl, U. Rant, Polymerase/DNA interactions and enzymatic activity: Multi-parameter analysis with electro-switchable biosurfaces. *Sci. Rep.* **5**, 12066 (2015).
39. H. Kong, R. B. Kucera, W. E. Jack, Characterization of a DNA polymerase from the hyperthermophile archaea *Thermococcus litoralis*. Vent DNA polymerase, steady state kinetics, thermal stability, processivity, strand displacement, and exonuclease activities. *J. Biol. Chem.* **268**, 1965–1975 (1993).
40. M. V. Akhterov, Y. Choi, T. J. Olsen, P. C. Sims, M. Iftikhar, O. T. Gul, B. L. Corso, G. A. Weiss, P. G. Collins, Observing lysozymes closing and opening motions by high-resolution single-molecule enzymology. *ACS Chem. Biol.* **10**, 1495–1501 (2015).
41. B. P. English, W. Min, A. M. Van Oijen, T. L. Kang, G. Luo, H. Sun, B. J. Cherayil, S. C. Kou, X. S. Xie, Ever-fluctuating single enzyme molecules: Michaelis-Menten equation revisited. *Nat. Chem. Biol.* **2**, 87–94 (2006).
42. N. Dan, Understanding dynamic disorder fluctuations in single-molecule enzymatic reactions. *Curr. Opin. Colloid Interface Sci.* **12**, 314–321 (2007).
43. B. I. Costescu, S. Sturm, F. Gräter, Dynamic disorder can explain non-exponential kinetics of fast protein mechanical unfolding. *J. Struct. Biol.* **197**, 43–49 (2017).
44. D. L. Floyd, S. C. Harrison, A. M. Van Oijen, Analysis of kinetic intermediates in single-particle dwell-time distributions. *Biophys. J.* **99**, 360–366 (2010).
45. S. Moran, R. X. F. Ren, E. T. Kool, A thymidine triphosphate shape analog lacking Watson-Crick pairing ability is replicated with high sequence selectivity. *Proc. Natl. Acad. Sci. U.S.A.* **94**, 10506–10511 (1997).
46. T. A. Kunkel, DNA replication fidelity. *J. Biol. Chem.* **279**, 16895–16898 (2004).
47. M. F. Juette, D. S. Terry, M. R. Wasserman, R. B. Altman, Z. Zhou, H. Zhao, S. C. Blanchard, Single-molecule imaging of non-equilibrium molecular ensembles on the millisecond timescale. *Nat. Methods* **13**, 341–344 (2016).
48. A. T. Raper, A. J. Reed, Z. Suo, Kinetic mechanism of DNA polymerases: Contributions of conformational dynamics and a third divalent metal ion. *Chem. Rev.* **118**, 6000–6025 (2018).
49. D. A. Carlin, S. Hapig-Ward, B. W. Chan, N. Damrau, M. Riley, R. W. Caster, B. Bethards, J. B. Siegel, Thermal stability and kinetic constants for 129 variants of a family 1 glycoside hydrolase reveal that enzyme activity and stability can be separately designed. *PLOS ONE* **12**, e0176255 (2017).
50. J. E. Diaz, C. S. Lin, K. Kunishiro, B. K. Feld, S. K. Avrantinis, J. Bronson, J. Greaves, J. G. Saven, G. A. Weiss, Computational design and selections for an engineered, thermostable terpene synthase. *Protein Sci.* **20**, 1597–1606 (2011).
51. M. B. Richardson, K. N. Gabriel, J. Garcia, S. Ashby, R. Dyer, J. Kim, C. Lau, J. Hong, R. J. Le Tourneau, S. Sen, D. Narel, B. B. Katz, J. W. Ziller, S. Majumdar, P. G. Collins, G. A. Weiss, Pyrocinchonimides conjugate to amine groups on proteins via imide transfer. *Bioconjug. Chem.* **31**, 1449–1462 (2020).

52. L. An, J. M. Owens, L. E. McNeil, J. Liu, Synthesis of nearly uniform single-walled carbon nanotubes using identical metal-containing molecular nanoclusters as catalysts. *J. Am. Chem. Soc.* **124**, 13688–13689 (2002).

Acknowledgments: We thank K. M. Pugliese and B. Boyanov from Illumina Inc. for suggestions on Taq variant design. We acknowledge the use of facilities and instrumentation at the Integrated Nanosystems Research Facility (INRF) in the Samueli School of Engineering at the University of California Irvine. **Funding:** This work was supported by the National Human Genome Research Institute of the National Institutes of Health, grant 1R01HG009188-01. K.N.G. was supported by a National Science Foundation Graduate Research Fellowship Program grant DGE-1839285. **Author contributions:** M.W.T., K.N.G., S.M., G.A.W., and P.G.C. designed the study; M.W.T., K.N.G., W.L., C.J.L., R.E.K., and S.M. developed methodology; K.N.G., J.K.K., S.C., R.E.K., J.T.P., and S.M. prepared enzymes and solutions; M.W.T., W.L., J.J.T., and D.G. prepared devices; M.W.T., J.J.T., and C.J.L. performed electrical measurements; M.W.T., K.N.G., J.J.T., C.J.L., and P.G.C. analyzed signals; and M.W.T., K.N.G., G.A.W., and P.G.C. wrote the manuscript. **Competing interests:** The authors declare that they have no competing interests. **Data and materials availability:** All data needed to evaluate the conclusions in the paper are present in the paper and/or the Supplementary Materials.

Submitted 8 July 2021
Accepted 21 January 2022
Published 11 March 2022
10.1126/sciadv.abl3522